



Fortnightly Variation of the Tsushima Warm Current on the Continental Shelf in the Southwestern Japan Sea

Tetsutaro Takikawa¹ , Akihiko Morimoto², Moeto Kyushima³, Kaoru Ichikawa⁴ , and Kei Yufu⁴

¹Nagasaki University, Nagasaki, Japan, ²Center for Marine Environmental Studies, Ehime University, Matsuyama, Japan, ³Institute for Space-Earth Environmental Research, Nagoya University, Nagoya, Japan, ⁴Research Institute for Applied Mechanics, Kyushu University, Fukuoka, Japan

Special Section:

Significant advances in ocean and climate sciences of the Pacific-Asian Marginal Seas

Key Points:

- Fortnightly variation of the Tsushima Warm Current on continental shelf
- Variation of the Tsushima Warm Current locally controlled by internal tides
- Relation between the Tsushima Warm Current and the bottom temperature front

Correspondence to:

T. Takikawa,
tetu@nagasaki-u.ac.jp

Citation:

Takikawa, T., Morimoto, A., Kyushima, M., Ichikawa, K., & Yufu, K. (2021). Fortnightly variation of the Tsushima Warm Current on the continental shelf in the southwestern Japan Sea. *Journal of Geophysical Research: Oceans*, 126, e2020JC017141. <https://doi.org/10.1029/2020JC017141>

Received 8 JAN 2021

Accepted 26 OCT 2021

Author Contributions:

Conceptualization: Tetsutaro Takikawa

Data curation: Tetsutaro Takikawa

Formal analysis: Tetsutaro Takikawa

Funding acquisition: Akihiko Morimoto

Investigation: Akihiko Morimoto, Moeto Kyushima, Kaoru Ichikawa, Kei Yufu

Methodology: Tetsutaro Takikawa

Project Administration: Akihiko Morimoto

Resources: Akihiko Morimoto

Supervision: Akihiko Morimoto

Visualization: Tetsutaro Takikawa

© 2021. The Authors.

This is an open access article under the terms of the [Creative Commons Attribution License](https://creativecommons.org/licenses/by/4.0/), which permits use, distribution and reproduction in any medium, provided the original work is properly cited.

Abstract The first and second branches of the Tsushima Warm Current flow on the continental shelf and along the shelf break/slope in the southwestern Japan Sea, respectively. The second branch corresponds to the offshore side of the bottom temperature front between the offshore cold and nearshore warm waters. Across the Tsushima Warm Current on the continental shelf and the shelf edge, five bottom-mounted ADCPs with temperature sensors were deployed between middle June and late July 2014. At the shelf edge, the bottom temperature varied with the diurnal tidal cycle. The offshore bottom cold-water intruded into the continental shelf region in conjunction with the fortnightly spring-neap (2-week) cycle which is the modulation of the diurnal K_1 and O_1 internal tides. The bottom temperature front and the first branch of the Tsushima Warm Current on the continental shelf intensified in response to the bottom cold-water intrusion.

Plain Language Summary The path of Tsushima Warm Current and its variation, in the southwestern Japan Sea after passing through the Tsushima Straits, are not well understood because of the mesoscale eddy activities and the strong tidal currents. In this study, using the observational time series data of the current profiles and the bottom temperatures, we found that the Tsushima Warm Current on the continental shelf intensified about every 2 weeks. The velocity enhancement was caused by the short-term variation and its modulation of the diurnal internal tides.

1. Introduction

The Tsushima Warm Current (TWC) flows from the East China Sea through the Tsushima Straits into the Japan Sea (Figure 1; e.g., Fukudome et al., 2010). Continental shelf, shallower than 200-m depth, extends from the East China Sea to the southwestern Japan Sea. The TWC typically divides into three branches flowing through two channels of the Tsushima Straits (e.g., Hase et al., 1999; Ito et al., 2014; Katoh, 1994; Kawabe, 1982). The first branch flows through the eastern channel as a coastal boundary current along the Japanese coast on the continental shelf. The second and third branches flow through the western channel along the continental shelf break/slope and along the Korean coast as a western boundary current (the East Korean Warm Current), respectively. Morimoto et al. (2009) revealed that the second branch of TWC exists throughout the year around the shelf edge in the southwestern Japan Sea, using shipboard acoustic Doppler current profiler (ADCP) data.

In the lower layer of the second TWC branch under the main thermocline/pycnocline, the dense cold water exists continuously from the offshore Japan Sea to the continental shelf slope between 150-m and 200-m isobaths (Kawabe, 1982). From the observational results of the relation between vertical temperature sections and shipboard ADCP currents, the horizontal temperature gradient at 100-m depth, near the bottom on the continental shelf, has been taken as an indicator of the current path of the TWC (e.g., Hase et al., 1999; Katoh, 1993, 1994). Although the second branch of TWC basically flows along the continental break/slope, the flow path would vary depending on the extent of the bottom cold water. On the east side of the Oki Island and the continental shelf break, Kaneda et al. (2019) reported the enhancement of the first TWC branch associated with the cold-water edge.

To focus on the short time scale, external tidal waves propagate from the East China Sea through the Tsushima Straits into the southwestern Japan Sea (e.g., Book et al., 2004; Odumaki, 1989). At the continental

Writing – original draft: Tetsutaro Takikawa
Writing – review & editing: Akihiko Morimoto, Kaoru Ichikawa

shelf-slope region around the northern entrance of the Tsushima Straits, Jeon et al. (2014) revealed internal tides with vertical motion of the thermocline above the bottom cold water, by hourly interval 25-hr long conductivity-temperature-depth (CTD) castings in early September 2012. The semidiurnal internal tides freely propagate farther in the Japan Sea (Jeon et al., 2014; Park & Watts, 2006). On the other hand, the diurnal tides are trapped along the lateral boundary of shelf slope as a double-Kelvin wave (also known as an interior shelf wave; Isoda & Murayama, 1993; Longuet-Higgins, 1968). According to the direct current measurements of Isoda and Murayama (1993), the amplitudes of the diurnal tidal current below the thermocline (140-m and 170-m depth) were much larger than those of the surface layer (50-m depth) at the shelf edge to slope, and varied with about 2-week cycle.

It is considered that the distribution of the offshore cold water would change with the vertical thermocline movement and mixing due to the internal tides. Although the cold-water distribution may affect the TWC, there is no previous observational study about the TWC variation associated with the internal tides in this region. In this paper, we elucidate that the TWC variations on the continental shelf of the southwestern Japan Sea associated with the internal tides at the shelf edge, using observational time series data of the bottom-mounted ADCP with temperature and pressure sensors. Especially, we focus on the relation between the first branch of the TWC and the bottom temperature front with the fortnightly (about 2 weeks) variation.

2. Observations and Data Processing

Across the TWC on the continental shelf of the southwestern Japan Sea (Figure 1) at the water depth range from 96 m (C1) to 163 m (C5), five bottom-mounted ADCPs (WH-Sentinel 300 kHz, Teledyne RD Instruments) with temperature and pressure sensors were deployed and recovered in middle June and late July 2014 (the total observation periods: 37–39 days), respectively, using the research vessel (R/V) *Shinsei-maru* of Japan Agency for Marine-Earth Science and Technology (JAMSTEC). The C5 and C1–C4 are located at the edge and interior of the continental shelf, respectively. The steep shelf break/slope is located on the north side of C5. The distance of each observation point (C2–C3, C3–C4, and C4–C5) is about 20 km except for nearshore C1. Temperature profiles at all stations were measured, at the times of deploying and recovering ADCPs, using a CTD (SBE911plus, Sea-Bird Electronics, Inc.) of R/V *Shinsei-maru*. Only these two times, we can compare the vertical sections of ADCP current with those of temperature.

The ADCP velocities and the bottom temperatures were recorded every 10-min ensemble average. The standard deviations of the current velocity for error index are $<0.5 \text{ cm s}^{-1}$. For data quality, we used the ADCP currents satisfied that percent good is greater than 75%. The percent good is the ratio of good pings per total pings for each ensemble average. The ADCPs with vertical intervals of 2 m (C1), 4 m (C2), and 8 m (C3–C5) obtained data below the surface 16-m (C1–C4) and 40-m (C5) depth to near the bottom. The ADCP currents and the bottom temperatures were averaged for 1 hr. Seven tidal constituents (Q_1 , O_1 , K_1 , μ_2 , N_2 , M_2 , and S_2) were removed from the ADCP data using harmonic analysis. In order to show the temporal variations longer than several days, the ADCP and the bottom temperature data were filtered with a 49-hr running mean. As the spatiotemporal variation of the surface TWC, we used the current velocities at 41-m depth (upper-most layer of C5) of all stations (C1–C5) after the linear vertical interpolation.

Pressure data loggers (Level TROLL 500, In-Situ Inc.) were attached to the bottom-mounted ADCPs at C3 and C5, to measure the time series of sea level. The water depth was recorded every 1-min. At C1, C2, and C4, we used the pressure data of the ADCP (WH-Sentinel) option sensor, where the ensemble average interval is 10 min. The sea level anomalies at each station were calculated by subtracting the mean water depth during the observation period. The data were averaged for 1 hr. Then the harmonic analysis was applied as same as the ADCP currents.

We downloaded the hourly wind data at Hagi (Figure 1), which is located near the Japanese coast, from the Japan Meteorological Agency, to compare with the variation of the ocean currents and the bottom temperatures. The 49-running mean was used to remove the short-term variations.

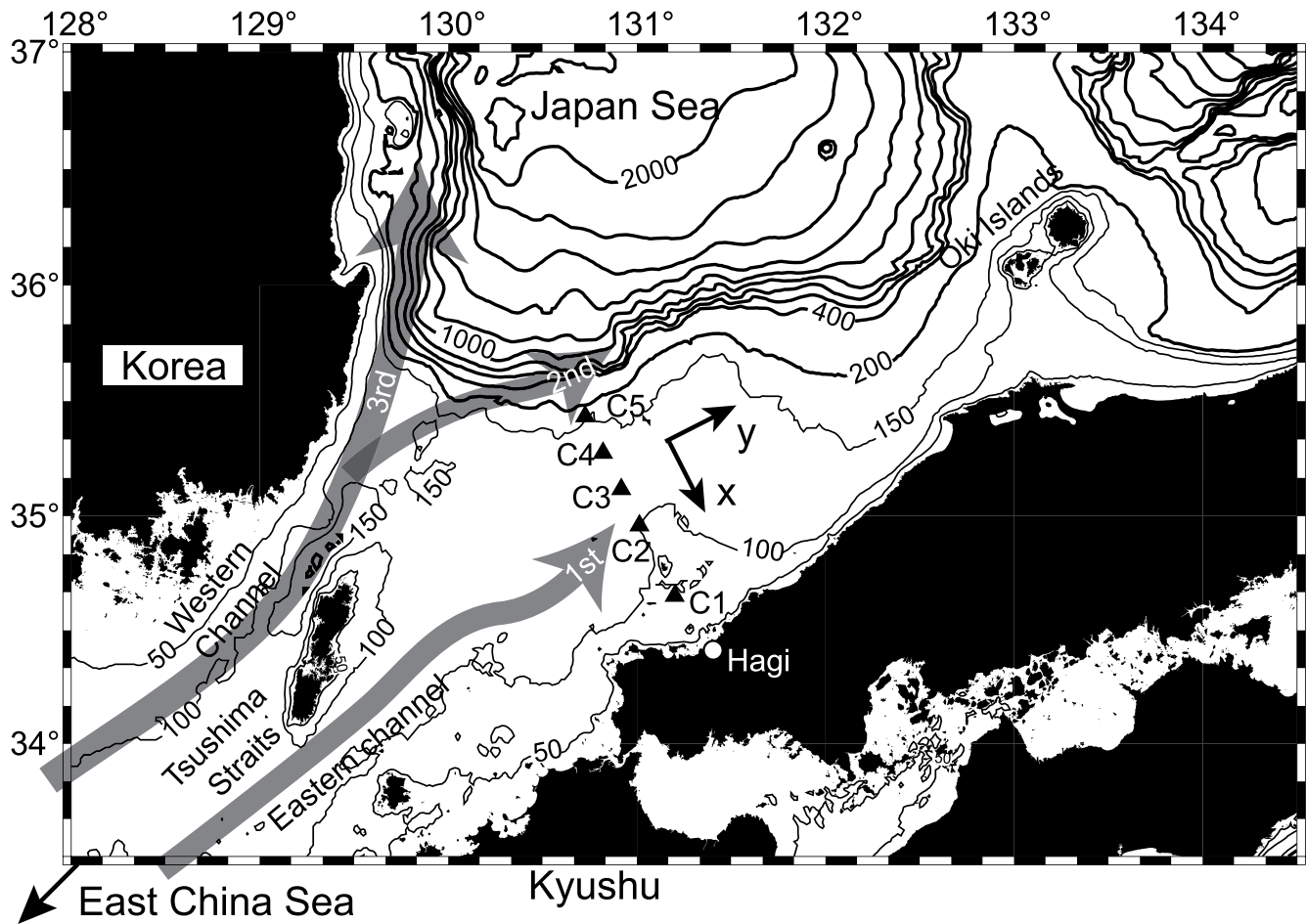


Figure 1. Map showing the locations of the bottom-mounted acoustic Doppler current profilers (ADCPs; triangles), the wind station (open circle, Hagi), and schematic view of the Tsushima Warm Current (gray arrows of the first, second, and third branches). Thin and thick contour lines indicate the bottom topography at 50 and 200-m intervals, respectively. The x-direction and y-direction are parallel and normal to the C1–C5 observation line, respectively, as shown on the map.

3. Results

The current profiles without tidal signals and the temperature sections along C1–C5, at the times of deploying and recovering ADCPs, are shown in Figures 2a and 2b. The structures of temperature and current of Figure 2a is similar to the observational results of Katoh (1993) near our study area. The northeastward to eastward strong current cores of the first and second TWC branches were found at C2 (26.5 cm s^{-1} at 41-m depth) and C4 (18.2 cm s^{-1} at 39-m depth), respectively, on June 17, 2014 (Figure 2a). Between the first and second branches at C3, the surface northeastward current was weak (9.1 cm s^{-1} at 37-m depth). On July 22, a single core of TWC broadly appeared along C2–C4. The maximum current velocity at C3 was 28.1 cm s^{-1} at 37-m depth (Figure 2b). The second branch of TWC might not have been distinguished from the first branch around C2–C3 or flowed north of C5 (out of observation area). The bottom cold waters $<4^\circ\text{C}$ extended from offshore side to the nearshore continental shelf both at the times of deploying and recovering ADCPs (Figures 2a and 2b). There was a sharp thermocline above the bottom cold water at C3–C5. Near the bottom along C3–C5, the westward countercurrents and weak flows were found on June 17 and July 22, 2014, respectively, associated with the bottom cold water.

The mean current profiles along the C1–C5 section during the observation period are shown in Figure 2c. The northeastward current core appeared at the surface of C2–C3 (Figure 2c), to be similar on July 22 (Figure 2b). The maximum current velocities at C2 and C3 were 31.1 cm s^{-1} (north-northeastward at 61-m depth) and 27.1 cm s^{-1} (east-northeastward at 27-m depth), respectively.

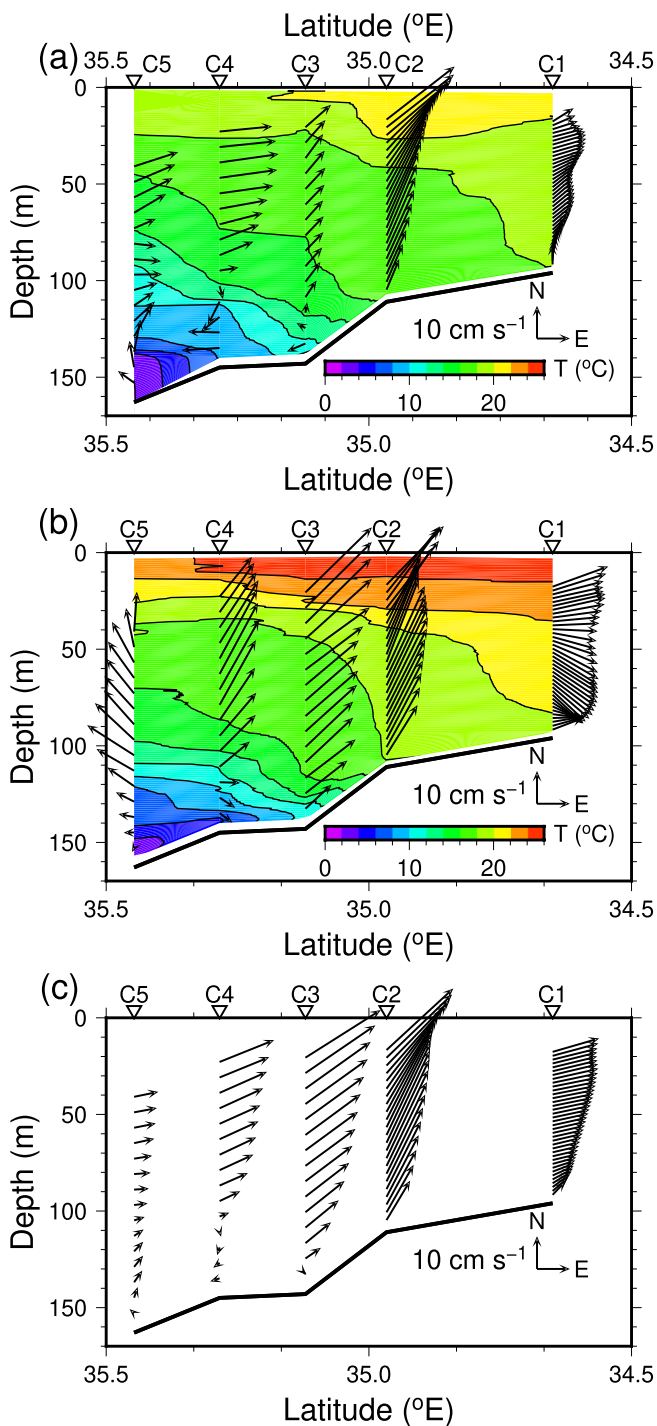


Figure 2. Temperature sections (colors) along C1–C5 at the times of (a) deploying and (b) recovering acoustic Doppler current profilers (ADCPs), and current velocity profiles (vectors) without tidal signals on (a) June 17 and (b) July 22, 2014. (c) The current vectors are averaged over the observation period.

Figure 3a shows the spatiotemporal variation of the observed bottom temperature, including the short-term variation, before the running mean. The warm water broadly distributed near the coast from C1 to C2. On the other hand, the bottom temperature in the offshore region at the continental shelf edge (C5) was lower than that of coastal region. There was a bottom temperature front between C2 and C5. It seems that the temperature front at the last half of the observation period was steeper than that of the first half.

Focusing on the short-term variations, the temperature of the bottom cold water at the offshore shelf edge (C5) varied with a period of about 1 day, considering the diurnal tides (Figure 3a). The amplitude of the temperature variation was large mainly on June 17, 29 and July 13 with roughly 2-week cycle. Hence, the large and small tidal variations of the bottom temperature are called spring and neap tides, respectively. The spatiotemporal variation of sea level anomaly also has a spring-neap tidal variation (Figure 4a). However, the semidiurnal amplitude of external tides was slightly larger than diurnal tides (Figures 4b and 4c). The coastal tidal amplitudes were larger than offshore tides. The tidal phases were almost same as in the whole observation line (C1–C5). The diurnal variation range of external tides at C5 (offshore shelf edge) was maximum on June 26 and July 11, which was leading to the bottom temperature variation (June 29 and July 13) by 2–3 days (Figures 3a and 4b). Figure 5 shows the power spectra of the bottom temperature and the sea level anomaly time series at C5. The significant two spectrum peaks of the sea level are found corresponding to the diurnal and semidiurnal periods. On the other hand, the semidiurnal signals of the bottom temperature are much weaker than diurnal ones. For detail, the diurnal peaks both of the bottom temperature and the sea level correspond to O_1 and K_1 tidal constituents.

Figure 3b shows the time-space diagram of the filtered bottom temperature with a 49-hr running mean, removing the tidal signals. The offshore temperature at C5 was minimum on June 22–23 (3.0°C), July 5 (2.6°C), and July 22 (2.0°C) in neap tide, and maximum on June 17 (4.4°C), June 29 (4.4°C), and July 12 (4.6°C) in spring tide. From neap to spring tide at C5 during June 26–29, the offshore cold water less than about 8°C spread southward and intruded into the continental shelf. Then the steep temperature front appeared between C2 and C3 after June 30.

To clarify the variations of the front, the bottom temperature gradient (nearshore-offshore) is shown in Figure 3c. The positive values indicate that the nearshore temperature was higher than the offshore one. The southward movements of the front were found not only during June 26–29 (i1) but also July 8–10 (i2), and at the end of observations around July 23 (i3). The propagation speeds of bottom water intrusion (gradients of lines i1 and i2) will be described later in the explanation of surface current fluctuations (Figure 6c). After the front movement, the temperature front between C2 and C3 intensified during July 2–8 and 15–19 (i1' and i2', temperature gradient $>0.45^\circ\text{C km}^{-1}$). At the almost same times, the temperature gradient between C3 and C4 became small or negative. The pair of high and low temperature gradients at the nearshore (C2–C3) and offshore (C3–C4) regions, respectively, was also found at the beginning of observations around June 16–22 (i0'). The enhancement of the nearshore front (C2–C3) accompanied with the bottom cold-water intrusion into the continental shelf occurred in a cycle of about 2 weeks.

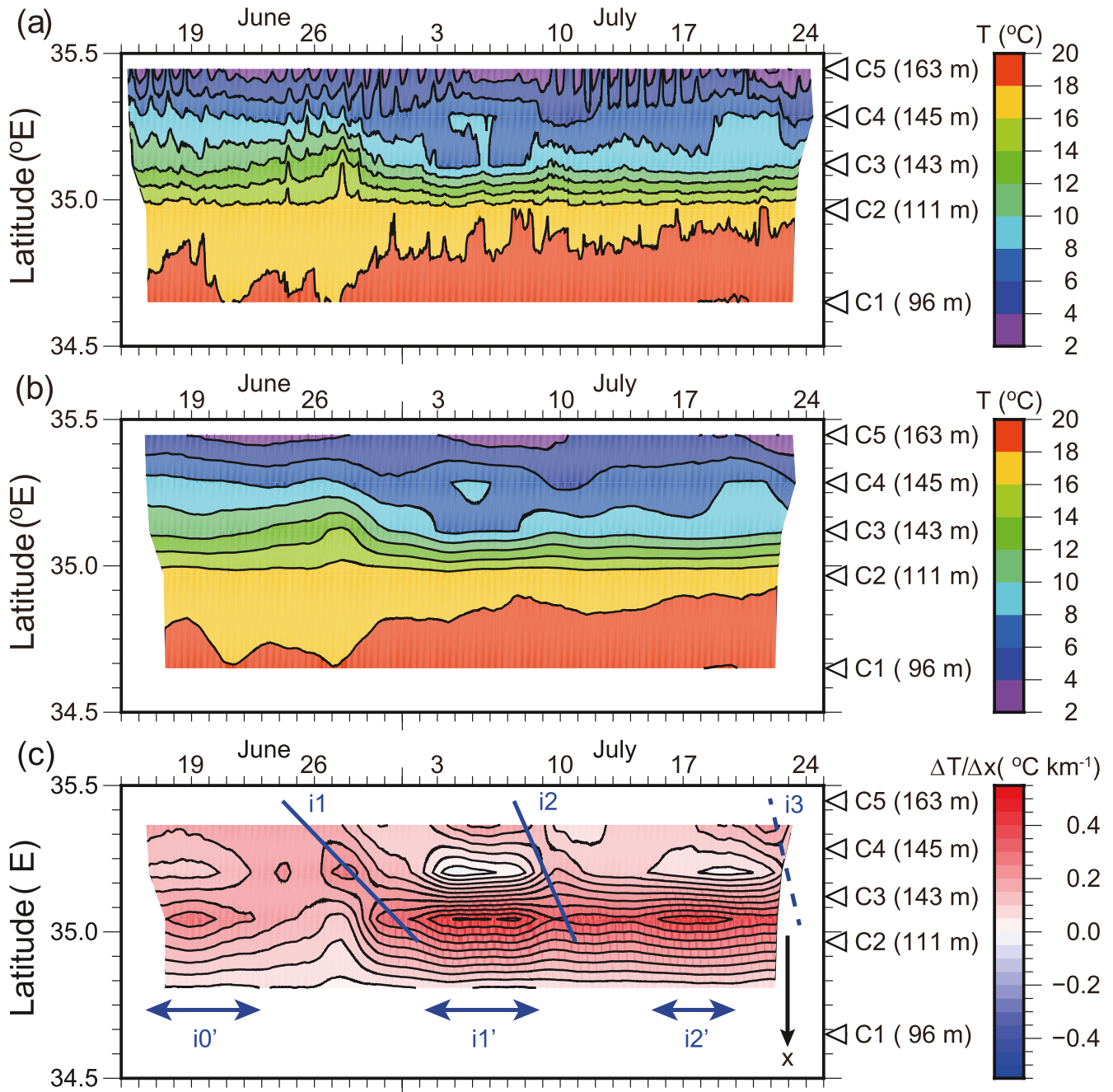


Figure 3. Spatiotemporal variability of the bottom temperature (a) without and (b) with a 49-hr running mean, and (c) the gradient in x -direction of (b). The x axis directs nearshore along the observation line. Water depth at each station is in parentheses. Front movements to nearshore indicate the lines of i_1 , i_2 , and i_3 in panel (c). The gradients of lines i_1 and i_2 will be derived later in Figure 6c. Pairs of strong (C2–C3) and weak (C3–C4) bottom temperature gradients appeared in the periods of i_0' , i_1' , and i_2' .

The current vectors at the sea bottom (the lowest layers of ADCP) are overlaid on the bottom temperature gradients (Figure 6a). Approaching spring tide (Figure 3a), the bottom temperature front moved to southward nearshore (i_1 and i_2 in Figure 3c). The current at the sea bottom also directed to south at the timing of the front intrusion (C3 and C4 in Figure 6a). The bottom current speeds of C4 at the i_1 and i_2 events were 5.1 and 8.0 cm s^{-1} , respectively.

The surface current vectors (41-m depth) are overlaid on the bottom temperature gradients (Figure 6b). The strong northeastward current of the first TWC branch was continuously found at C2, and its mean current

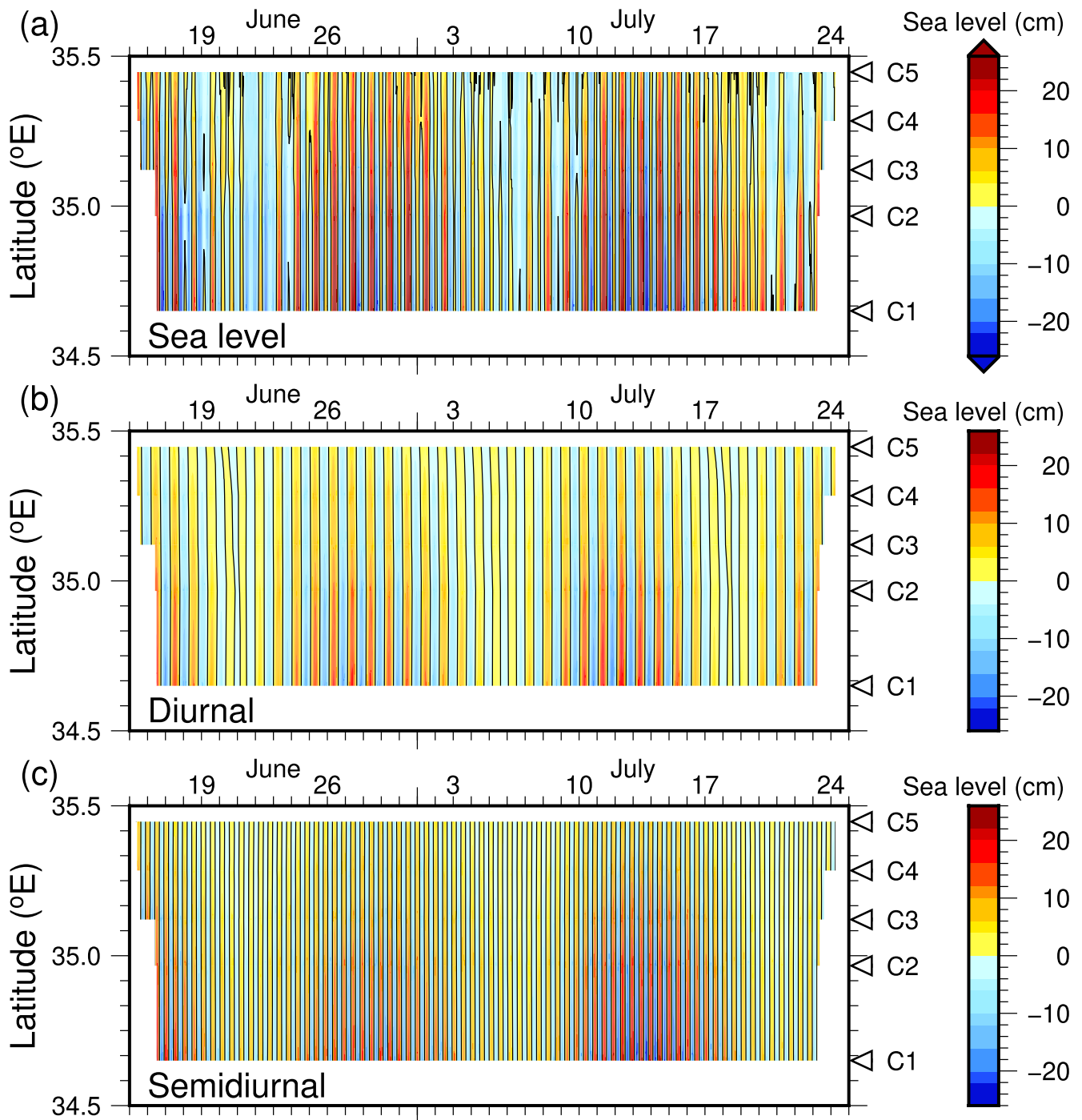


Figure 4. Spatiotemporal variability of (a) the sea level anomaly estimated from the bottom pressure data, (b) the diurnal tides (Q_1 , O_1 , and K_1), and (c) the semidiurnal tides (μ_2 , N_2 , M_2 , and S_2). The contour lines indicate zero level.

speed was 28.1 cm s^{-1} . It seems that the current vectors at C2–C4 varied with about 2-week cycle. The north-eastward currents intensified in conjunction with the southward movement of the bottom temperature front. When the offshore bottom temperature was the same or warmer than the nearshore one between C3 and C4 (temperature gradient $<0.1^\circ\text{C km}^{-1}$ on July 2–8 and 15–22), the surface currents at C4 and C3 were southwestward and weakening, respectively.

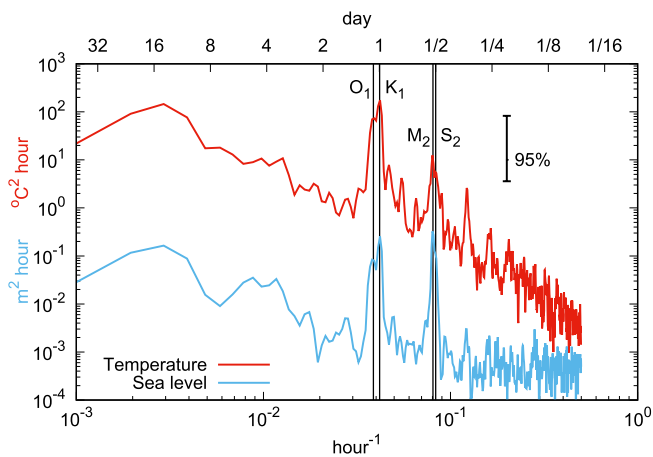


Figure 5. Spectra of the bottom temperature (red line) and the sea level (blue line) at C5. The vertical lines indicate the frequencies (or periods) of O_1 , K_1 , M_2 , and S_2 constituents, from left to right.

Figure 6c shows the time-space diagram of the east-northeastward surface current velocities normal to the observation line (y -direction in Figure 1). Between C2 and C5 using four-point data (blue circles in Figure 6c), the regression lines i1 and i2 were linearly fitted from the scatter plots between observation points along the x axis and times taking the maximum east-northeastward velocity. Here, the correlation coefficients (or the root mean squares) of i1 and i2 were 0.99 and 0.96 (or 0.46 and 0.39 days), respectively. The estimated propagation speeds of the current fluctuations along i1 and i2 were 7.7 km day^{-1} (8.9 cm s^{-1}) and 17.0 km day^{-1} (19.7 cm s^{-1}), respectively. The exact same lines of i1 and i2 were drawn in the time-space diagram of the bottom temperature (Figure 3c). The propagation speeds of bottom cold-water intrusion (Figure 3c) corresponded well with those of the current fluctuation (gradients of lines i1 and i2 in Figure 6c).

The velocity enhancements occurred at almost same time when the near-shore bottom temperature gradients became steeper (Figures 3c and 6c). After the front movement to nearshore and the current accelerations (i1 and i2), the east-northeastward currents increased again (i1' and i2' in Figure 6c). These velocity increments only occurred near the first branch of TWC core (C2 and C3), but were not found offshore (C4 and C5). On the other hand, the east-northeastward currents were weak during i1' and i2' at C4 in Figure 6c. Soon after the current enhancement at C3 and weakening at C4, the pairs of strong and weak bottom temperature gradients appeared at C2–C3 and C3–C4, respectively (i1' and i2' in Figure 3c).

4. Summary and Discussion

The diurnal signal of the bottom temperature in the offshore region at the continental shelf edge (C5) varied with the fortnightly spring-neap tidal cycle (Figure 3a). It is considered that the spring-neap variation were caused by the modulation of the K_1 and O_1 tidal components (Figure 5). The spring-neap cycle of K_1 (23.934-hr period) and O_1 (25.819-hr period) is 13.66 days. According to Isoda and Murayama (1993), the diurnal tidal currents were more remarkable than the semidiurnal ones at the lower layer on the shelf edge to slope in the southwestern Japan Sea. The diurnal internal tides trapped on the shelf slope region mentioned above is called the double-Kelvin wave (Longuet-Higgins, 1968).

In spring tide, the bottom temperature increased at the shelf edge (C5 in Figures 3a and 3b), probably due to the vertical mixing with the upper warm water by the internal tides. The sharp thermocline was found above the bottom cold water (Figure 2). Although Jeon et al. (2014) shows the vertical displacement of thermocline caused by the semidiurnal internal tides using hourly temperature profile data at about 75 km east from C5, the diurnal internal tides also exist according to the numerical ocean model results (Chae et al., 2018). It is considered that the bottom cold-water intruded into the continental shelf when the thermocline was lifted by the internal tidal wave.

The numerical and observational studies of the internal tidal mixing between the continental shelf and basin were conducted in the Bering Sea (e.g., Tanaka et al., 2013), even though it is far from the southwestern Japan Sea. They suggested that the diurnal topographic trapped waves along the shelf slope contribute the vertical mixing and the energy dissipation on the bottom near the shelf break although the internal semidiurnal tidal waves freely propagate from the shelf break into the basin along the ray paths. In the southwestern Japan Sea, the mechanism of the bottom cold-water intrusion associated with the internal tide and mixing remains for future study.

The main thermocline/pycnocline intersects the continental shelf slope between 150 and 200-m isobaths (Kawabe, 1982) and forms the bottom temperature front. According to Katoh (1993) and the first half of the observation period in this study, the bottom temperature front was observed around 120–140 m water depth, and the first and second branches of the TWC, respectively, flowed nearshore and offshore sides on the continental shelf. It has been considered that the second branch of TWC flows just on the offshore side of the

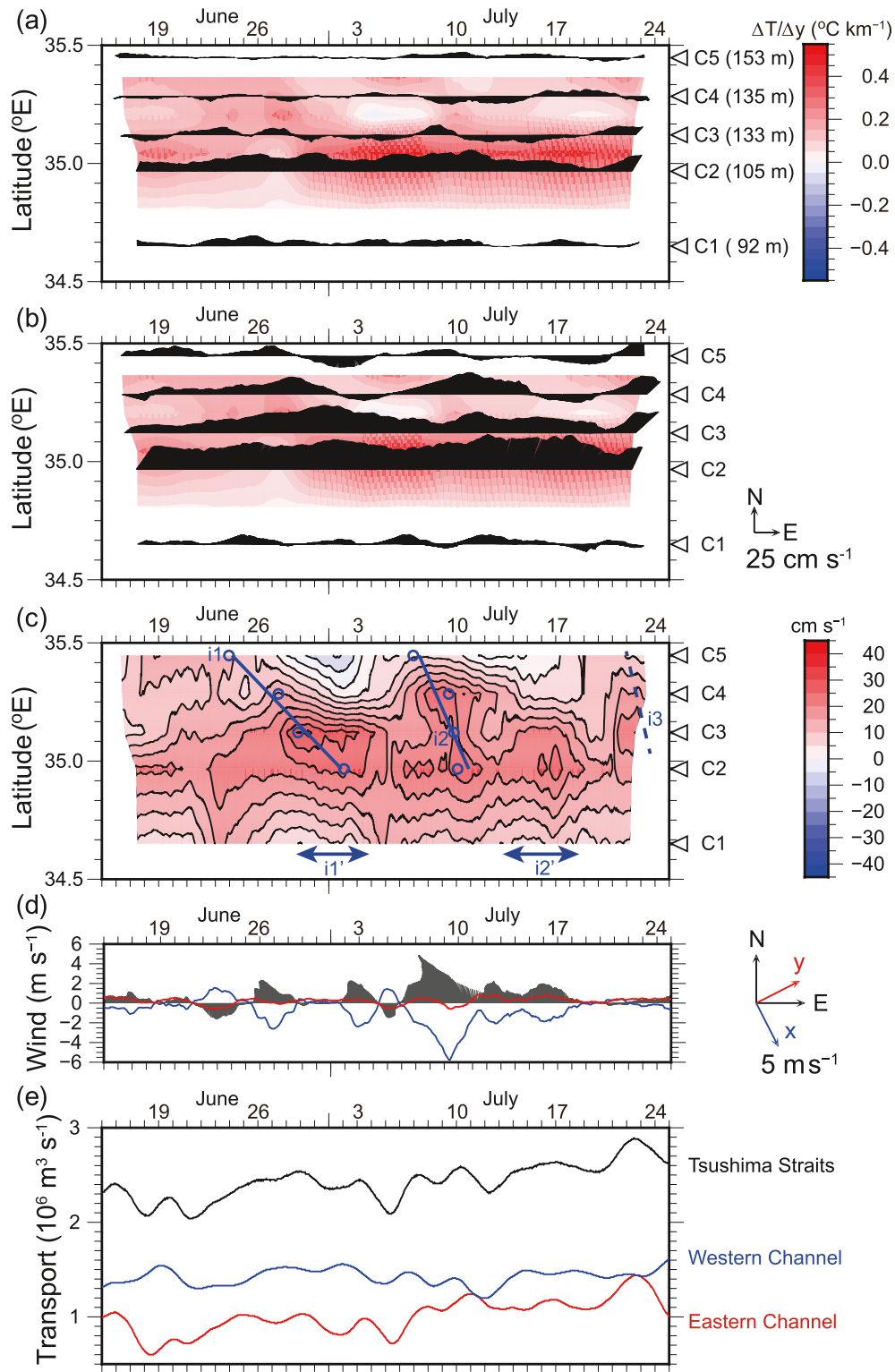


Figure 6. Spatiotemporal variability of the (a) bottom (the lowest layers of acoustic Doppler current profiler (ADCP)), (b) surface (41-m depth) current vectors without tidal signals, (c) surface current velocity component of y-direction, (d) time series of the wind vectors at Hagii, and (e) volume transport through the Tsushima Straits (black line), the western (blue line) and eastern (red line) channels with 49-hr running mean. (a) Observation depth of the bottom currents at each station is in parentheses. (a and b) The colors indicate the bottom temperature gradient in Figure 3c. (c) Blue circles indicate the date when the y-ward velocity had the maximum at each station and event. Blue regression lines at each event (i1 and i2) were estimated from blue points. The remarkable changes indicate i1' and i2' after the front movements i1 and i2. (d) Blue and red lines indicate the wind speeds of x-direction and y-direction, respectively.

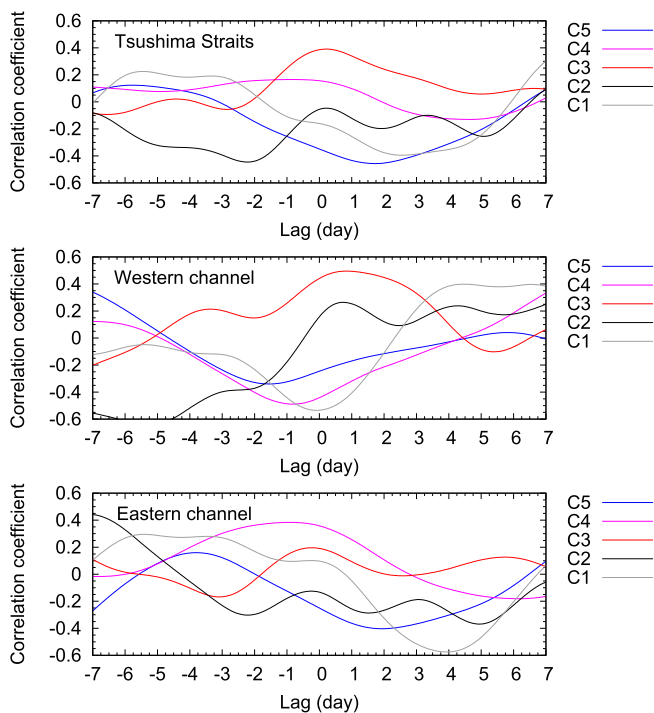


Figure 7. (a) Lag correlations between the volume transport through the Tsushima Straits and the y -ward currents at C1–C5 after the 49-hr running mean, and same except for the (b) western and (c) eastern channels. The positive values of the time lag (horizontal axis) indicate that the throughflow transports were leading to the currents at C1–C5.

bottom temperature front, which is almost coincident with the temperature front at about 100-m depth and the isobath of the shelf break/slope (e.g., Hase et al., 1999). In this study case, the bottom temperature front at the last half of the observation period was found more nearshore than that of the first half (Figures 2a and 2b) because of the bottom cold-water intrusion from offshore (Figure 3). The second branch of TWC might have joined with the first branch (Figure 2b). When the bottom cold-water intruded into the continental shelf region with the fortnightly variation, associated with the spring-neap cycle of the internal diurnal tides, the velocity of the first TWC branch on the continental shelf intensified simultaneously (Figure 6b). After the front and current enhancements caused by the bottom cold-water intrusion, the current velocity of the first TWC branch and its bottom temperature gradient increased again ($i1'$ and $i2'$ in Figure 6c). It might be needed to consider the frontal wave or shear instability of the TWC front (Takikawa et al., 2012).

As a possibility of the atmospheric forcing to the ocean, the time series of wind near the observation area (Hagi in Figure 1) is shown in Figure 6d. The north-northwest and south-southeasterly fluctuations were dominant. These wind directions were almost parallel to the C1–C5 line and almost normal to the TWC flow. The south-southeasterly winds (negative direction of x axis) were maxima on June 26, July 2, 9, 12, and 16, where the period was not 2 weeks but roughly 1 week, except for July 12. The strong wind on July 9 was due to the Typhoon Neoguri which was moving eastward while weakening from the East China Sea to Kyushu in Japan.

When the strength of the background mean TWC varies, it is considered that the thermocline/pycnocline moves via geostrophic adjustment. In this way, the bottom cold water might intrude into the continental shelf region. As an indicator of the background current strength, the volume transport through the Tsushima Straits, which is the upstream inflow condition of the TWC into the Japan Sea, can be estimated from sea level difference (Takikawa & Yoon, 2005). The 49-hr running means of volume transports through both the western and eastern channels of the Tsushima Straits are shown in Figure 6e. To focus on the fortnightly variation, the volume transports including the small signals were minimum on June 21, July 4–5 and 19–20 although the variations of the several days period were dominant. The linear correlation analyses were performed using the possible combinations between the volume transports (Tsushima Straits, the western and eastern channels) and the east-northeastward currents (C1–C5), considering time lag within ± 7 days (Figure 7). However, we did not find a remarkable correlation between the eastern channel throughflow and the currents in this study area. Although the highest correlation coefficient 0.50 is obtained between the western channel throughflow and the current at C3, there is no positive correlation between the western channel and the offshore area (C4 and C5) in this study within ± 4 -day lag. As mentioned above, it is considered that the fortnightly variation of the first TWC branch was caused by the internal tides in the interior of the Japan Sea because the surface current fluctuations clearly propagated from offshore shelf edge (C5) to nearshore on the continental shelf (C3–C2) as shown in Figures 6b and 6c.

In this study, we considered the diurnal tidal signals as a short time variation. In this area, the inertia period is about 21 hr which is close to the diurnal cycle. The near-inertial internal waves (18–19-hr period) appeared after the strong wind stress (Igeta et al., 2009). It is interesting to consider the interaction between the TWC and the short-term variation, including not only tides but also atmospheric wind forcing (Kaneda et al., 2017; Takikawa et al., 2017), for future observations. However, in this observation period, we could not find a remarkable variation caused by wind forcing (Figure 6d). According to Moon et al. (2009) and Takikawa et al. (2017), in this observation area, the alongshore wind might be more effective to the ocean current than the cross-shore one.

Data Availability Statement

The observed data are archived in Japan Oceanographic Data Center (JODC: <https://www.jodc.go.jp>).

Acknowledgments

This study was discussed at the Pacific-Asian Marginal Seas (PAMS) Meeting and the research meetings of the Joint and Collaborative Research Program of the Institute of Low Temperature Science, Hokkaido University and Research Institute for Applied Mechanics, Kyushu University. The authors thank the scientific party, captain and crews of R/V *Shinsei-maru* (KS-14-09 and KS-14-09), especially Dr. Masashi Ito of Nagoya University at that time. The authors also wish to thank the Japan Meteorological Agency for providing the wind data. This work was supported by the JSPS KAKENHI Grant Nos. JP25247076, JP26450254, and JP19H05698. Two anonymous reviewers provided comments that helped improve the manuscript.

References

- Book, J. W., Pistek, P., Perkins, H., Thompson, K. R., Teague, W. J., Jacobs, G. A., et al. (2004). Data assimilation modeling of the barotropic tides in the Korea/Tsushima Strait. *Journal of Oceanography*, *60*, 977–993. <https://doi.org/10.1007/s10872-005-0006-6>
- Chae, J.-Y., Jeon, C., Park, S. J., & Park, J.-H. (2018). Behavior of diurnal internal waves in the southwestern East/Japan Sea. *Journal of Coastal Research*, *85*, 486–490. <https://doi.org/10.2112/SI85-098.1>
- Fukudome, K., Yoon, J.-H., Ostrovskii, A., Takikawa, T., & Han, I.-S. (2010). Seasonal volume transport variation in the Tsushima Warm Current through the Tsushima Straits from 10 years of ADCP observations. *Journal of Oceanography*, *66*, 539–551. <https://doi.org/10.1007/s10872-010-0045-5>
- Hase, H., Yoon, J.-H., & Koterayama, W. (1999). The current structure of the Tsushima Warm Current along the Japanese Coast. *Journal of Oceanography*, *55*, 217–235. <https://doi.org/10.1023/A:1007894030095>
- Igeta, Y., Kumaki, Y., Kitade, Y., Senjyu, T., Yamada, H., Watanabe, T., et al. (2009). Scattering of near-inertial internal waves along the Japanese coast of the Japan Sea. *Journal of Geophysical Research*, *114*, C10002. <https://doi.org/10.1029/2009JC005305>
- Isoda, Y., & Murayama, T. (1993). Diurnal shelf waves off Hamada on San'in Coast. *Journal of Oceanography*, *49*, 71–88. <https://doi.org/10.1007/BF02234010>
- Ito, M., Morimoto, A., Watanabe, T., Katoh, O., & Takikawa, T. (2014). Tsushima Warm Current paths in the southwestern part of the Japan Sea. *Progress in Oceanography*, *121*, 83–93. <https://doi.org/10.1016/j.pocean.2013.10.007>
- Jeon, C., Park, J.-H., Varlamov, S. M., Yoon, J.-H., Kim, Y. H., Seo, S., et al. (2014). Seasonal variation of semidiurnal internal tides in the East/Japan Sea. *Journal of Geophysical Research: Oceans*, *119*, 2843–2859. <https://doi.org/10.1002/2014JC009864>
- Kaneda, A., Ayukawa, K., Hirose, N., Senjyu, T., Kumaki, Y., Igeta, Y., et al. (2019). Intensification of current in coastal waters around Cape Echizen in summer. *Journal of Oceanography*, *75*, 157–169. <https://doi.org/10.1007/s10872-018-0492-y>
- Kaneda, A., Ayukawa, K., Hirose, N., Tsuzuki, J., Kumaki, Y., Senjyu, T., et al. (2017). Sudden strong current generated by an eddy in the eastern part of Wakasa Bay, Japan. *Journal of Oceanography*, *73*, 181–192. <https://doi.org/10.1007/s10872-016-0395-8>
- Katoh, O. (1993). Detailed current structures over the continental shelf off the San'in Coast in summer. *Journal of Oceanography*, *49*, 1–16. <https://doi.org/10.1007/BF02234004>
- Katoh, O. (1994). Structure of the Tsushima Current in the Southwestern Japan Sea. *Journal of Oceanography*, *50*, 317–338. <https://doi.org/10.1007/BF02239520>
- Kawabe, M. (1982). Branching of the Tsushima Current in the Japan Sea, Part I. Data analysis. *Journal of the Oceanographical Society of Japan*, *38*, 95–107. <https://doi.org/10.1007/BF02110295>
- Longuet-Higgins, M. S. (1968). Double Kelvin waves with continuous depth profiles. *Journal of Fluid Mechanics*, *34*(1), 49–80. <https://doi.org/10.1017/S002211206800176X>
- Moon, J.-H., Hirose, N., Yoon, J.-H., & Pang, I.-C. (2009). Effect of the along-strait wind on the volume transport through the Tsushima/Korea Strait in September. *Journal of Oceanography*, *65*, 17–29. <https://doi.org/10.1007/s10872-009-0002-3>
- Morimoto, A., Isoda, Y., Tameishi, T., & Moriwaki, S. (2009). Seasonal variation in Tsushima Warm Current paths over the shelf off the San'in coast, Japan. *Continental Shelf Research*, *29*, 1437–1447. <https://doi.org/10.1016/j.csr.2009.03.017>
- Odamaki, M. (1989). Tides and tidal currents in the Tsushima Strait. *Journal of the Oceanographical Society of Japan*, *45*, 65–82. <https://doi.org/10.1007/BF02108795>
- Park, J.-H., & Watts, D. R. (2006). Internal tides in the southwestern Japan/East Sea. *Journal of Physical Oceanography*, *36*(1), 22–34. <https://doi.org/10.1175/JPO2846.1>
- Takikawa, T., Onitsuka, G., Fukudome, K., Yoon, J.-H., & Morimoto, A. (2012). Seasonal variation of counterclockwise eddies downstream of the Tsushima Islands. *Progress in Oceanography*, *105*, 30–37. <https://doi.org/10.1016/j.pocean.2012.04.006>
- Takikawa, T., Watanabe, T., Senjyu, T., & Morimoto, A. (2017). Wind-driven intensification of the Tsushima Warm Current along the Japanese coast detected by sea level difference in the summer monsoon of 2013. *Continental Shelf Research*, *143*, 217–277. <https://doi.org/10.1016/j.csr.2016.06.004>
- Takikawa, T., & Yoon, J.-H. (2005). Volume transport through the Tsushima Straits estimated from sea level difference. *Journal of Oceanography*, *61*, 699–708. <https://doi.org/10.1007/s10872-005-0077-4>
- Tanaka, T., Yasuda, I., Tanaka, Y., & Carter, G. S. (2013). Numerical study on tidal mixing along the shelf break in the Green Belt in the southeastern Bering Sea. *Journal of Geophysical Research: Oceans*, *118*, 6525–6542. <https://doi.org/10.1002/2013JC009113>